



1

2 New insights on the prevalence of drizzle in marine stratocumulus  
3 clouds based on a machine learning algorithm applied to radar Doppler  
4 spectra

5

6 Zeen Zhu<sup>1</sup>, Pavlos Kollias<sup>1,2</sup>, Edward Luke<sup>2</sup> and Fan Yang<sup>2</sup>

7

8 <sup>1</sup>School of Marine and Atmospheric Sciences, Stony Brook University, Stony Brook, NY, USA

9 <sup>2</sup> Environmental and Climate Sciences Dept, Brookhaven National Laboratory Upton, NY, USA

10

11 *Correspondence to:* Zeen Zhu ([zeen.zhu@stonybrook.edu](mailto:zeen.zhu@stonybrook.edu))

12

13 **Abstract**

14

15 The detection of the early growth of drizzle particles in marine stratocumulus clouds is important  
16 for studying the transition from cloud water to rainwater. Radar reflectivity is commonly used to  
17 detect drizzle; however, its utility is limited to larger drizzle particles. Alternatively, radar Doppler  
18 spectrum skewness has proven to be a more sensitive quantity for detection of drizzle embryos.  
19 Here, a machine-learning (ML) based technique that uses radar reflectivity and skewness for  
20 detecting small drizzle particles is presented. Aircraft in-situ measurements are used to develop  
21 and validate the ML algorithm. The drizzle detection algorithm is applied to three Atmospheric  
22 Radiation Measurement (ARM) observational campaigns to investigate the drizzle occurrence in  
23 marine boundary layer clouds. It is found that drizzle is far more ubiquitous than previously  
24 thought, the traditional radar reflectivity-based approach significantly underestimates the drizzle  
25 occurrence, especially in thin clouds with liquid water path lower than  $50 \text{ gm}^{-2}$ . Furthermore, the  
26 drizzle occurrence in marine boundary layer clouds differs among three ARM campaigns,  
27 indicating that the drizzle formation which is controlled by the microphysical process is regime  
28 dependent. A complete understanding of the drizzle distribution climatology in marine  
29 stratocumulus clouds calls for more observational campaigns and continuing investigations.

30

31



32 **1. Introduction**

33

34 Clouds play an important role in the climate system and the accurate representation of their  
35 properties and feedbacks in Global Circulation Models (GCM) is essential for performing reliable  
36 future climate prediction (Cess et al., 1989; Bony et al., 2006; Vial et al., 2013). Among all the  
37 cloud types, marine stratocumulus is an important cloud type covering approximately 20% of the  
38 Earth's surface (Warren et al., 1986, 1988; Wood, 2012). Marine stratocumulus clouds  
39 significantly modulate the Earth's energy budget: on one hand, stratocumulus with high albedo  
40 strongly reflect incoming solar radiation back to space; on the other hand, as stratocumulus clouds  
41 have similar temperature with surface, they emit comparable amount of longwave radiation as the  
42 surface and do not significantly affect the infrared radiation emitted to space. Thus, overall the  
43 stratocumulus have a strong cooling effect to the climate system. (Hartmann et al., 1992). It is  
44 estimated that only a small increase of the marine stratocumulus coverage can compensate for the  
45 increased temperature induced by the greenhouse gas effect (Randall et al., 1984). Despite the  
46 considerable influence on the climate, large uncertainties persist in the representation of marine  
47 stratocumulus in GCMs due to a lack of understanding of the cloud properties and the associated  
48 processes. (Stephens, 2005; Klein et al., 2017) One important issue is the underrepresentation of  
49 the transition from cloud water to rainwater, i.e. the autoconversion process. (Stephens et al.,  
50 2010; Michibata and Takemura, 2015). (Paluch and Lenschow, 1991; Yamaguchi et al., 2017). A  
51 misrepresentation of the autoconversion process in GCM's can affect not only the hydrological  
52 cycle but also generate compensating errors in the aerosol-cloud interactions (Michibata and  
53 Suzuki, 2020).

54

55 The core component of autoconversion is the production and growth mechanisms of drizzle drops.  
56 Drizzle, by definition, refers to liquid droplets with a diameter between 40  $\mu\text{m}$  and 500  $\mu\text{m}$  (Wood,  
57 2005a; Glienke et al., 2017; Zhang et al., 2021). Drizzle is frequently observed in the warm cloud  
58 system and can modulate the cloud organizational structure and the boundary layer system in  
59 several ways: the drizzle production process tends to warm the cloud layer and stabilize the  
60 boundary layer, which reduces cloud top entrainment and produces thicker clouds (Wood,  
61 2012; Nicholls, 1984; Ackerman et al., 2009); the coalescence process can reduce cloud droplet  
62 concentration and cause cloud precipitation (Wood, 2006); furthermore, drizzle also plays a critical



63 role in the formation of the open-cell pattern of stratocumulus (Wang and Feingold, 2009; Feingold  
64 et al., 2010) and tends to promote the stratocumulus to cumulus transitions process (Paluch and  
65 Lenschow, 1991; Yamaguchi et al., 2017).

66

67 Despite the importance role of drizzle plays on the marine boundary layer, a thorough  
68 understanding of its existence is incomplete due to the detection limitation. Historically, in-situ  
69 and remote sensing measurements have been used to detect drizzle in cloud (Leon et al.,  
70 2008; Wood, 2005a; Wu et al., 2015; Yang et al., 2018; VanZanten et al., 2005). In-situ  
71 microphysical probes can provide size-resolved microphysical properties, importantly, Drop Size  
72 Distribution (DSD), from which drizzle drops can be easily identified according to their definition.  
73 The disadvantage of in-situ observations is the limited datasets collected during field campaigns,  
74 making it challenging to provide long term statistical analyses. Millimeter-wavelength radar,  
75 commonly known as cloud radar, is widely used for cloud/drizzle detections (Kollias et al., 2007a).  
76 The total received backscatter power of droplets is converted to radar reflectivity factor, which is  
77 independent of the radar wavelength in the cloud/drizzle regime, and is proportional to the sixth  
78 power of the diameter of the particles in the radar resolution volume<sup>1</sup>. Compared with cloud  
79 droplets, drizzle drops have larger diameters, which produce greater reflectivity, and this signature  
80 is widely used to differentiate cloud/drizzle signals. Different reflectivity thresholds, ranging from  
81 -15dBZ to -20dBZ, have been applied in previous studies to identify drizzle existence (Frisch et  
82 al., 1995; Liu et al., 2008; Comstock et al., 2004). Nevertheless, this reflectivity-based technique  
83 has obvious drawbacks. As reflectivity is the summation of the backscattered power from all the  
84 droplets in a radar volume, the reflectivity threshold can detect the presence of drizzle drops only  
85 when their contribution to the total radar backscatter exceeds that of the cloud droplets. More  
86 specifically, when cloud droplets dominate the reflectivity signal, even if drizzle drops exist, they  
87 fail to be detected as the total reflectivity is usually lower than -20 dBZ; this indicates that the  
88 reflectivity-based technique is unable to detect small drizzle particles (Kollias et al., 2011b).

89

90 Besides reflectivity, another radar observed quantity which is sensitive to the presence of drizzle  
91 is the skewness of the radar Doppler spectrum (hereafter skewness). Skewness is the third moment  
92 of the radar-observed Doppler spectrum and is a measure of the asymmetry of the spectrum. For

---

<sup>1</sup> It is noted that attenuation is not considered in this study.



93 cloud droplets, Doppler spectra are on average symmetric with skewness equal to zero; as drizzle  
94 drops grow and start falling, their terminal velocity is recorded in the fast-falling part of the  
95 Doppler spectra, which has greater backscatter power than the power contributed by cloud droplets,  
96 leading to asymmetric spectra with a non-zero skewness (Kollias et al., 2011b; Luke and Kollias,  
97 2013). The capability of using skewness to detect early drizzle development stages was  
98 demonstrated in Acquistapace et al. (2019). In Acquistapace et al. (2019) a threshold of the  
99 skewness is used as part of the detection algorithm. Considering the noisiness in the estimation of  
100 the third moment of the radar Doppler spectrum, the use of a fixed threshold value can lead to  
101 considerable misclassifications. Here, a supervised Machine Learning (ML) algorithm is used to  
102 provide a more robust detection of drizzle particles in warm stratiform clouds. First, in-situ DSD  
103 measurements are used as input to a sophisticated radar Doppler spectrum simulator that can  
104 accurately represent the performance of the ARM profiling cloud radars in estimating the  
105 corresponding radar-observed reflectivity and skewness. Next, the ML algorithm is trained from  
106 2 months of in-situ observations to generate a classification model; the classification results from  
107 one case study will be presented and compared against the in-situ measurements. Finally,  
108 comprehensive datasets from three ARM observational campaigns are used to investigate drizzle  
109 occurrence and demonstrate the omnipresence of drizzle in marine stratocumulus clouds.

110

## 111 **2. Instruments and Data**

112

113 The data used in this study are collected from three observatories operated by the U.S. Department  
114 of Energy's Atmospheric Radiation Measurement (ARM) facility. The Eastern North Atlantic  
115 (ENA) is a permanent observational site established on Graciosa Island in the Azores archipelago  
116 in 2013 as representative of a maritime environment. The Aerosol and Cloud Experiments in the  
117 Eastern North Atlantic (ACE-ENA) field campaign was conducted in the vicinity of the ENA site  
118 from June 2017 to February 2018. The Gulfstream-1 aircraft was deployed during ACE-ENA to  
119 provide in-situ measurements. The Marine ARM GPCI Investigation of Clouds (MAGIC)  
120 campaign was based on a mobile observatory facility traversing between Los Angeles, California,  
121 and Honolulu, Hawaii, from October 2012 to September 2013. Measurements of Aerosols,  
122 Radiation, and Clouds over the Southern Ocean (MARCUS) was a field campaign conducted from  
123 October 2017 to April 2018 along the route between Hobart, Australia, and the Antarctic. All of



124 the observational campaigns were equipped with a variety of instruments which provide  
125 comprehensive datasets being used in this study.

126

127 The primary instrument being used in this study is the cloud radar: a Ka-Band ARM Zenith Radar  
128 (KAZR) was operated at ENA and MAGIC and a W-Band ARM Cloud Radar (WACR) was used  
129 during MARCUS. The KAZR and WACR are both vertically pointing with 30 m range resolution;  
130 the temporal resolution of the WACR and KAZR used at ENA is 2 s, while the temporal resolution  
131 of the KAZR used for MAGIC is 0.36 s. To make the observations comparable, radar moments  
132 from MAGIC are averaged over 2 s to be consistent with the ones collected at ENA and MARCUS.  
133 Radar reflectivity and Doppler skewness are obtained from the Microscale Active Remote Sensing  
134 of Clouds (MicroARSCL) product (Kollias et al., 2007b). Radar reflectivity at ENA and MAGIC  
135 is calibrated with surface-based measurements of the raindrop PSD using a disdrometer (Gage et  
136 al., 2000; Kollias et al., 2019). At MARCUS, a disdrometer is not suitable for radar calibration thus  
137 instead we follow Mace et al. (2021) by adding 4.5 dB to the reflectivity for WACR calibration.  
138 In addition, a ceilometer and microwave radiometer (MWR) are used to estimate cloud base height  
139 and liquid water path (LWP). The time resolution of the MWR and ceilometer are 10 s and 15 s  
140 respectively. Besides the surface-based observations, in-situ measurements from ACE-ENA  
141 during the intensive observation period 1 (IOP1) which was conducted from 21 June to 20 July in  
142 2017 are also used in this study. The DSD of hydrometeors with diameter ranging from 1.5  $\mu\text{m}$  to  
143 9075  $\mu\text{m}$  are characterized using combined measurements from the fast cloud droplet probe  
144 (FCDP), 2-dimensional stereo probe (2D-S) and high-volume precipitation spectrometer (HVPS-  
145 3). Liquid water content is measured using a multi-element water content system and a Gerber  
146 probe.

147

### 148 **3. Methodology**

149

150 As Doppler skewness is a sensitive indicator of weak drizzle signals, the focus of the methodology  
151 is to synthesize this quantity with reflectivity to construct a robust drizzle detection algorithm.  
152 Thus, the key issue lies in the challenging task of determining the appropriate reflectivity/skewness  
153 combination to identify drizzle signals. Here we address this problem in a novel way: first we  
154 identify the existence of cloud/drizzle based on in-situ observed DSDs; then a well-established



155 Doppler spectrum simulator is applied to emulate the radar observed spectrum for the given DSD  
156 and estimate the corresponding reflectivity and skewness. Finally, the resulting collection of well-  
157 defined cloud/drizzle datasets is trained by a machine learning algorithm to resolve the drizzle  
158 identification function.

159

### 160 **3.1 Doppler spectrum simulation**

161

162 According to previous studies, liquid droplets with diameter exceeding 40  $\mu\text{m}$  are defined to be  
163 drizzle (Wood, 2005a; Zhang et al., 2021). We follow this definition to classify the in-situ observed  
164 DSD: cloud/drizzle are defined by the maximum diameter in the DSD being smaller/larger than  
165 40  $\mu\text{m}$ . Example DSDs of cloud-only and mixed cloud-drizzle conditions are shown in Fig. 1a and  
166 Fig. 1c. Next, the Doppler spectrum simulator developed by Kollias et al. (2011a) is applied to  
167 generate the radar-observed Doppler spectrum based on the in-situ DSD. The associated simulator  
168 parameters are set as follows: Doppler spectra are generated with 256 FFT bins and a Nyquist  
169 velocity of  $\pm 6$  m/s, which correspond to the KAZR configuration operated by ARM (Kollias et  
170 al., 2016); turbulence broadening ( $\sigma_t$ ) is set as 0.2 m/s which is obtained from local observations:  
171 for radar observation with reflectivity smaller than -20 dBZ, Doppler spectra width is mainly  
172 contributed by turbulence and can be used to estimate  $\sigma_t$ . The KAZR-observed spectral width  
173 collected from the ACE-ENA IOP1 indicate that the mean value of the  $\sigma_t$  is estimated as 0.2 m/s  
174 (Fig. S1). Finally, radar noise is simulated by adding random perturbation to the Doppler spectra;  
175 positive velocity indicates downward motion. A detailed description of the Doppler spectrum  
176 simulator application is found in Zhu et al. (2021). Once a spectrum is generated, a post-processing  
177 algorithm (Kollias et al., 2007b) is used to eliminate noise (Hildebrand and Sekhon, 1974) and to  
178 estimate the Doppler moments, i.e. reflectivity and skewness. To demonstrate that the simulator  
179 can represent radar observations, the simulated reflectivity and skewness are compared with  
180 KAZR observations (Fig. S2) and shows consistent ranges and distribution pattern, indicating that  
181 the simulated radar moments are capable to represent the real observation signal. The relatively  
182 large fraction of the in-situ measurements with dBZ > -20 in Fig. S2 is likely caused by the  
183 different observational strategies between in-situ and KAZR measurements (Wang et al., 2016).

184



185 Fig. 1b and 1d show examples of the simulated Doppler spectra along with the estimated  
186 reflectivity and skewness for a cloud-only and mixed cloud-drizzle DSD. It is noticed for the  
187 drizzle case (Fig. 1d), reflectivity is well below the conventional threshold (-20 ~ -15 dBZ) used  
188 for drizzle detection and is unable to discriminate it from the cloud-only case (Fig. 1b). Skewness,  
189 however, shows a significant difference between drizzle (0.5) and cloud (0), emphasizing the  
190 importance of including skewness as an additional indicator for drizzle detection.

191

### 192 **3.2 Machine Learning algorithm application**

193

194 From the IOP1 of ACE-ENA, 6000 in-situ observed DSDs (2000 for cloud-only and 4000 for  
195 mixed cloud-drizzle) are selected from the cloudy samples defined as having liquid water content  
196 larger than  $0.01 \text{ gm}^{-3}$  (Zhang et al., 2021). For each DSD, the spectrum simulator is applied to  
197 estimate the reflectivity and Doppler skewness. The distribution of these two quantities for all the  
198 selected datasets is shown in Fig. 2. It shows that drizzle with positive skewness tends to be  
199 associated with reflectivity lower than -20 dBZ. For reflectivity ranging from -35 to -25 dBZ and  
200 skewness around zero, the drizzle signal overlaps with cloud; this region represents the early stage  
201 of drizzle initiation with low reflectivity and indistinguishable skewness features compared with  
202 cloud signals.

203

204 In order to determine the classification boundary to distinguish cloud/drizzle categories (i.e.  
205 red/blue points in Fig. 2), we apply a supervised machine learning algorithm which is widely used  
206 in classification-related problems, the Support Vector Machine (SVM) (Cortes and Vapnik,  
207 1995; Vapnik et al., 1997). SVM handles complicated data classification tasks by solving  
208 optimization relationships and finding the optimal classification equations in the feature space.  
209 There are three reasons to use SVM in this study: 1) SVM is nonparametric and thus does not  
210 require specification or assumption of the classification equation; 2) By applying the appropriate  
211 kernel, SVM can generate a non-linear classification boundary to classify non-linearly separable  
212 datasets; 3) The decision boundary resolved by SVM will separate the categories with maximum  
213 distance; this is a distinctive feature of the SVM algorithm which is extensively used in a variety  
214 of areas (Ma and Guo, 2014).

215



216 For the collected cloud/drizzle datasets, 80% of them are used for training, and the remain 20%  
217 for validation. Inputs to the SVM are Doppler skewness and reflectivity, where the reflectivity  
218 from -50 dBZ to 0 dBZ is normalized from -1 to 0; the output is classified as either cloud (0) or  
219 drizzle (1). Here the Radial Basis Function (RBF) with two tuning parameters,  $\Gamma$  and  $C$ , is used as  
220 the SVM kernel (Keerthi and Lin, 2003). The RBF kernel is one of the most widely used kernels  
221 due to its similarity to the Gaussian distribution. The  $\Gamma$  parameter determines the curvature of the  
222 decision boundary with a high value indicating more curvature for capturing the complexity of the  
223 dataset;  $C$  is a regularization parameter to set the classification accuracy versus the maximization  
224 of the decision function margin; a lower  $C$  leads to a larger margin, and a simpler decision function  
225 at the cost of training accuracy. Following Davis and Goadrich (2006), we use precision/recall to  
226 evaluate the performance of the classification outcome. In this study, precision refers to the number  
227 of correct drizzle detections divided by total drizzle detections reported by the SVM, and recall  
228 refers to the number of the correct drizzle detections divided by the number of true drizzle  
229 occurrences in dataset. Different combinations of RBF parameters with  $\Gamma$  ranging from 1 to 500  
230 and  $C$  from 1 to 1000 are applied, with the classification outcome shown in Table 1. Here we  
231 choose  $\Gamma = 50$  and  $C = 1$  as the preferred parameters to produce classification results with precision  
232 and recall as 98% and 85%, respectively. That is, for the cloud-drizzle dataset collected at ACE-  
233 ENA, at most, 85% of the drizzle can be detected by the algorithm and among the detection  
234 outcomes, 98% are true drizzle signals.

235

236 The resolved classification boundary is shown as the black line in Fig. 2. We can see the algorithm  
237 reasonably separates the cloud/drizzle clusters; the resolved skewness threshold being used to  
238 distinguish cloud/drizzle is around  $\pm 0.2$ , and the maximum reflectivity used for classification is -  
239 20dBZ. These values are consistent with previous studies (Frisch et al., 1995; Liu et al.,  
240 2008; Kollias et al., 2011b; Acquistapace et al., 2019). We further estimate the cumulative  
241 distribution function (CDF) of the correctly detected drizzle samples as a function of dBZ from  
242 the ML technique (magenta solid line in Fig. 2) and from the traditional method with reflectivity  
243 threshold ranging from -20 to -15 dBZ. (magenta shading in Fig. 2). It is noticed that drizzle can  
244 be detected with dBZ  $< -30$  from the ML method; this value is significantly lower than for  
245 traditional thresholds in use. The ML method is more sensitive to the weak drizzle signals than the  
246 dBZ thresholds that have been proposed. Specifically, compared to the ML technique, 35% and



247 21% of the drizzle are missed by the reflectivity threshold approach when using dBZ >-20 and  
248 dBZ >-15, respectively. Another important implication of this result is that dBZ >-15 is  
249 traditionally applied by CloudSat to identify light rain incidence (Haynes et al., 2009); here we  
250 demonstrate that a more robust threshold is likely to be much lower.

251

252 Besides the encouraging performance of the ML technique, some noticeable issues can be  
253 identified: 1) Compared with the true CDF of the drizzle fraction (dotted magenta line in Fig. 2),  
254 20% of drizzle is undetected. This missing drizzle subset, as explained previously by the  
255 overlapping area, is composed of tiny drizzle embryos that have yet to develop distinctive features  
256 compared with their cloud counterparts. 2) Another issue is the unrealistic broadening of the  
257 classification boundary for reflectivity lower than -35dBZ; this issue is related to the kernel being  
258 applied in the SVM algorithm. Since drizzle rarely exists below -35 dBZ, this issue will not affect  
259 the classification performance as far as we are concerned.

260

## 261 **4.Results**

262

263 The ML-based drizzle detection algorithm is applied to the dataset collected at three ARM  
264 observatories. First, an example case is presented for which aircraft observations are available and  
265 the corresponding in-situ measurements are used to demonstrate the performance of the algorithm.  
266 Then, the drizzle occurrence on classified stratocumulus clouds at ENA, MARCUS and MAGIC  
267 observatories are presented; the differences of the drizzle occurrence from the proposed machine  
268 learning based algorithm (hereafter MLA) and the traditional dBZ-based algorithm (hereafter  
269 dBZA) are compared to indicate that drizzle occurrence in stratocumulus clouds is far more  
270 frequent than has been previously suggested. For the dBZA, we use reflectivity >-17 dBZ for  
271 drizzle identification, while the application of other thresholds ranging from -20 to -15 dBZ did  
272 not affect the results as discussed.

273

### 274 **4.1 Single cloud layer case**

275

276 For the selected case (Fig. 3), a thin cloud layer with thickness around 150m is identified. Cloud  
277 signals is very weak with 99% of reflectivity lower than -17 dBZ. However, considerable large



278 skewness values shown in Fig. 3b indicates the presence of the drizzle particles. The classification  
279 results from the MLA classification are shown in Fig. 3c, it can be seen that drizzle is omnipresent  
280 and spread throughout the cloud layer, mixed with cloud-only detections.

281

282 Here the in-situ observed DSD is used to verify the MLA detection. On June 30th, 2017, aircraft  
283 measurements were conducted from 09:27 to 13:16 UTC. We constrained the in-situ  
284 measurements to be within 20 km of the ENA observatory (Fig. 4). Considering that the average  
285 in-cloud wind speed is 3.7 m/s, the distance of 20 km is equivalent to around 1.5 hour of KAZR  
286 observations; thus, the radar measurements from 08:00 to 13:30 UTC are selected to match the  
287 aircraft observations. We assume the signal of the drizzle/cloud occurrence collected from the  
288 in-situ measurements can be used to verify the drizzle presence observed from KAZR. For the  
289 selected period, drizzle occurrence is 47% from the MLA detections and 65% from the in-situ  
290 observations. The 18% of the missing drizzle by MLA is largely attributed to the “overlapping  
291 area” shown in Fig. 2 indicating the early stage of drizzle embryos which are indistinguishable  
292 from cloud droplets. Nevertheless, this comparison provides strong evidence that drizzle is widely  
293 present in the cloud layer for the selected case and demonstrates that the classification results from  
294 MLA are reliable. Contrastingly, negligible drizzle signals (0.05%) are detected with the  
295 reflectivity-based (dBZ >-17) technique.

296

#### 297 **4.2 Drizzle occurrence at ARM campaigns**

298

299 During the operational periods of ACE-ENA, MARCUS and MAGIC, single-layer marine  
300 stratocumulus clouds are selected with cloud top temperature greater than 0 °C and cloud top  
301 height lower than 4000 m. The moving standard deviation of cloud top height within 30-minutes  
302 ( $\sigma$ ) is calculated and profiles with  $\sigma$  larger than 200 m are excluded to reject non-stratocumulus-  
303 type clouds. LWP retrievals are biased when MWR is wet; thus, radar profiles with their lowest  
304 range gates containing hydrometeor detections are considered to be precipitation and are removed  
305 from the analysis. A complete list of the days being used is shown in Table 2. In total, 204, 72, and  
306 215 hours of radar observation were selected from the ACE-ENA, MARCUS and MAGIC  
307 campaigns.

308



309 In order to composite cloud layers with different thickness, cloud height is normalized between 0  
310 to 1 as:

$$311 \quad h = \frac{H - H_b}{H_t - H_b}$$

312

313 Where  $H$  is the physical height of a given radar gate,  $H_t$  and  $H_b$  is the cloud top and base height.  
314  $h=0$  represents cloud base and  $h=1$  indicates cloud top.

315

316 Drizzle occurrence is calculated as the number of drizzle detections divided by the total observed  
317 signals in each normalized height bin (0.1) and LWP bin ( $50 \text{ g m}^{-2}$ ). The drizzle occurrence being  
318 detected from both methods at the three ARM observatories are shown in Fig. 5. For all the  
319 observational site/campaigns, drizzle is more likely to occur as LWP increases. This tendency  
320 holds true despite the drizzle detection method being used. However, for each observational  
321 campaign, drizzle occurrence detected from MLA (Fig. 5 a, b, c) is always larger than from dBZA  
322 (Fig. 5 d, e, f). This difference becomes significant especially for thin clouds with low LWP: when  
323 LWP is under  $50 \text{ g m}^{-2}$ , or equivalently, cloud thickness is less than 200 m (Fig. 6), drizzle  
324 occurrence being detected from dBZA is around 0.1 while it is 0.4~0.5 from MLA. This result  
325 clearly indicates that the traditional drizzle detection method based on a reflectivity threshold  
326 significantly underestimates the true drizzle occurrence, especially in thin cloud layers. To  
327 quantitatively describe the detection performance, we estimate the relative percentage difference  
328 of the drizzle detections between two methods as follows:

$$329 \quad P_{LWP} (\%) = \frac{N_{MLA,LWP} - N_{dBZA,LWP}}{N_{MLA,LWP}} * 100$$

330 Where  $N_{MLA,LWP}$  and  $N_{dBZA,LWP}$  indicate the number of the drizzle detection by MLA and dBZA  
331 respectively for a given LWP category. The results (Fig. 7a) indicate that when LWP is smaller  
332 than  $50 \text{ g m}^{-2}$ , which frequently occurs under the ENA and MAGIC campaigns (Fig. 7b), 90% of  
333 drizzle are missed by dBZA at ENA and MARCUS, and 60 % of drizzle is undetected at MAGIC  
334 compared with MLA. An application of a relative lower reflectivity threshold with  $dBZ < -20$ , to  
335 some degree, mitigate the missing drizzle detections compared with MBL, but still with 50~80%  
336 of the drizzle being undetected (shading area in Fig. 7a).

337



338 Besides the considerable drizzle signals missed by dBZA, another implication to be noted is the  
339 difference of drizzle distribution among the three ARM campaigns. Specifically, large drizzle  
340 fractions tend to occur in the upper part of cloud at ENA and in the lower parts of cloud at  
341 MARCUS and MAGIC (Fig. 5). When compared with MLA, the missing drizzle detections based  
342 on dBZA are much more significant for ENA/MARCUS than for MAGIC (Fig. 7a). The different  
343 drizzle distribution pattern suggests that clouds among these three campaigns might have different  
344 microphysical properties and processes that controls the drizzle initiation. For instance, the  
345 contrasting thermodynamics environment among the ARM campaigns with low/high temperature  
346 and humidity at MARCUS/MAGIC might leads to different autoconversion process which control  
347 the drizzle formation. In particular, we suspect that a more humid environment under MAGIC will  
348 benefits the generation of larger cloud droplets compared with the other campaigns (Laird et al.,  
349 2000;Zhou et al., 2015). Fig. 8 supports this hypothesis by showing that the mean cloud reflectivity  
350 at MAGIC is 8dB larger than it is at the other two campaigns for LWP smaller than  $100 \text{ gm}^{-2}$ . The  
351 relatively large dBZ for small LWP, to some degree, mitigates the underrepresented drizzle  
352 detection by the reflectivity-based method.

353

## 354 5. Conclusion and Discussion

355

356 Building on the concept that radar Doppler spectra skewness is more sensitive to drizzle presence,  
357 a new method of detecting drizzle in marine boundary clouds is presented. In-situ observed DSDs  
358 are used to unambiguously classify cloud and drizzle particles; then, a radar Doppler spectra  
359 simulator is applied to estimate the expected radar-observed reflectivity and skewness. Extensive  
360 datasets collected from the ACE-ENA campaign are trained via the ML-based algorithm to  
361 optimally determine a classification equation of cloud/drizzle. The proposed algorithm is validated  
362 by the in-situ measurements to successfully detect weak drizzle signals, which are completely  
363 missed by the traditional reflectivity-based technique.

364

365 The drizzle/cloud classification outcome of a thin cloud layer observed on June 30, 2017 at ENA  
366 was presented to show the performance of the detection algorithm. It was found that even for thin  
367 cloud with thickness less than 150 m, a significant amount of drizzle already exists; this  
368 classification result is further verified by the in-situ observations. Furthermore, a statistical



369 analysis compares the drizzle occurrence from two detection methods at the ACE-ENA, MARCUS  
370 and MAGIC field campaigns. The results indicate that drizzle is ubiquitous in cloud layers and its  
371 existence has been significantly underestimated by conventional reflectivity-based methods,  
372 especially in thin cloud layers. The drizzle occurrence and vertical structure differ among the three  
373 campaigns, indicating that drizzle formation and distribution in marine stratocumulus clouds might  
374 be regime dependent, determined by microphysical and dynamical process in the local region. In  
375 this study, data from the three observational campaigns are used to explore the drizzle frequency  
376 of marine stratocumulus in middle/high latitude regions; however, it is quite possible that the  
377 drizzle occurrence from other locations might differ from the presented results. A complete  
378 understanding of the drizzle climatology in marine stratocumulus clouds calls for more campaign  
379 observations and continuing investigations.

380

381 The results in this study provide a new perspective for viewing drizzle existence in radar  
382 observations with the hope of shedding light on several critical topics in the warm cloud studies:  
383 1) In most microphysics retrieval algorithms, the existence of drizzle particles is determined by a  
384 reflectivity threshold. However, this study shows the presence of significant drizzle drops during  
385 low reflectivity conditions (lower than -20 dBZ) and a lack of considering this may lead to a certain  
386 degree of the retrieval uncertainty; 2) Drizzle production mechanisms are widely regarded as a  
387 critical missing piece of the puzzle in warm cloud research (Takahashi et al., 2017). Particularly,  
388 the parameterization schemes of the autoconversion/accretion processes in numerical models have  
389 large variations among each other, leading to significant uncertainty in future climate predictions  
390 (Michibata and Suzuki, 2020; Wood, 2005b). The results presented in this study can be used to  
391 verify the proposed parameterization schemes by comparing the drizzle climatology. 3)  
392 Furthermore, the novel utilization of in-situ and remote sensing synthesis of observations presented  
393 in this study yields insights on the potential of combined multi-platform observations to investigate  
394 the microphysical processes in warm clouds.

395

396

397

398

399



400  
401 **Data availability:** The ARM observational datasets are available at the ARM Data Center. The  
402 KAZR data (kazrge) can be accessed via <http://dx.doi.org/10.5439/1025214>. The ceilometer  
403 dataset (ceil) can be accessed via <http://dx.doi.org/10.5439/1181954>. The retrieved LWP product  
404 (mwrret2turn) can be accessed via <http://dx.doi.org/10.5439/1566156>. The in-situ observation  
405 during the ACE-ENA campaign can be accessed via  
406 <https://adc.arm.gov/discovery/#/results/iopShortName::aaf2017ace-ena>.

407  
408

409 **Supplement:** The supplement related to this article is available online at:

410  
411

412 **Author contributions:** Z.Z. designed the methodology and performed the analysis. P.K.  
413 contributed the design of the study. E.L. provide the MicroARSCL datasets. F.Y. assisted in the  
414 interpretation of results. Z.Z. prepared the manuscript with contributions from all co-authors.

415

416 **Competing interests:** The authors declare that they have no conflict of interest.

417

418 **Acknowledgments:** We would also like to acknowledge the data support provided by the  
419 Atmospheric Radiation Measurement (ARM) Program sponsored by the U.S. Department of  
420 Energy.

421

422 **Financial support:** Z. Z.'s contributions were supported by the U.S. Department of Energy (DOE)  
423 ASR ENA Site Science award. P. K., E. L. and F. Y. were supported by the US Department of  
424 Energy (DOE) Atmospheric System Research Program under contract DE-SC0012704.

425  
426  
427



## 428 References

429

- 430 Ackerman, A. S., VanZanten, M. C., Stevens, B., Savic-Jovicic, V., Bretherton, C. S., Chlond, A., Golaz,  
431 J.-C., Jiang, H., Khairoutdinov, M., and Krueger, S. K.: Large-eddy simulations of a drizzling,  
432 stratocumulus-topped marine boundary layer, *Monthly Weather Review*, 137, 1083-1110, 2009.
- 433 Acquistapace, C., Löhnert, U., Maahn, M., and Kollias, P.: A new criterion to improve operational  
434 drizzle detection with ground-based remote sensing, *Journal of Atmospheric and Oceanic*  
435 *Technology*, 36, 781-801, 2019.
- 436 Bony, S., Colman, R., Kattsov, V. M., Allan, R. P., Bretherton, C. S., Dufresne, J.-L., Hall, A.,  
437 Hallegatte, S., Holland, M. M., Ingram, W., Randall, D. A., Soden, B. J., Tselioudis, G., and Webb,  
438 M. J.: How well do we understand and evaluate climate change feedback processes?, *Journal of*  
439 *Climate*, 19, 3445-3482, 10.1175/jcli3819.1, 2006.
- 440 Cess, R. D., Potter, G., Blanchet, J., Boer, G., Ghan, S., Kiehl, J., Le Treut, H., Li, Z.-X., Liang, X.-Z.,  
441 and Mitchell, J.: Interpretation of cloud-climate feedback as produced by 14 atmospheric general  
442 circulation models, *Science*, 245, 513-516, 1989.
- 443 Comstock, K. K., Wood, R., Yuter, S. E., and Bretherton, C. S.: Reflectivity and rain rate in and  
444 below drizzling stratocumulus, *Quarterly Journal of the Royal Meteorological Society: A journal*  
445 *of the atmospheric sciences, applied meteorology and physical oceanography*, 130, 2891-2918,  
446 2004.
- 447 Cortes, C., and Vapnik, V.: Support-vector networks, *Machine learning*, 20, 273-297, 1995.
- 448 Davis, J., and Goadrich, M.: The relationship between Precision-Recall and ROC curves,  
449 *Proceedings of the 23rd international conference on Machine learning*, 2006, 233-240,
- 450 Feingold, G., Koren, I., Wang, H., Xue, H., and Brewer, W. A.: Precipitation-generated oscillations  
451 in open cellular cloud fields, *Nature*, 466, 849-852, 2010.
- 452 Frisch, A., Fairall, C., and Snider, J.: Measurement of stratus cloud and drizzle parameters in ASTEX  
453 with a Ka-band Doppler radar and a microwave radiometer, *Journal of the Atmospheric Sciences*,  
454 52, 2788-2799, 1995.
- 455 Gage, K. S., Williams, C. R., Johnston, P. E., Ecklund, W. L., Cifelli, R., Tokay, A., and Carter, D. A.:  
456 Doppler radar profilers as calibration tools for scanning radars, *Journal of Applied Meteorology*,  
457 39, 2209-2222, 2000.
- 458 Glienke, S., Kostinski, A., Fugal, J., Shaw, R., Borrmann, S., and Stith, J.: Cloud droplets to drizzle:  
459 Contribution of transition drops to microphysical and optical properties of marine stratocumulus  
460 clouds, *Geophysical Research Letters*, 44, 8002-8010, 2017.
- 461 Hartmann, D. L., Ockert-Bell, M. E., and Michelsen, M. L.: The effect of cloud type on Earth's  
462 energy balance: Global analysis, *Journal of Climate*, 5, 1281-1304, 1992.
- 463 Haynes, J. M., L'Ecuyer, T. S., Stephens, G. L., Miller, S. D., Mitrescu, C., Wood, N. B., and Tanelli,  
464 S.: Rainfall retrieval over the ocean with spaceborne W-band radar, *Journal of Geophysical*  
465 *Research: Atmospheres*, 114, 2009.
- 466 Hildebrand, P. H., and Sekhon, R.: Objective determination of the noise level in Doppler spectra,  
467 *Journal of Applied Meteorology*, 13, 808-811, 1974.
- 468 Keerthi, S. S., and Lin, C.-J.: Asymptotic behaviors of support vector machines with Gaussian  
469 kernel, *Neural computation*, 15, 1667-1689, 2003.



- 470 Klein, S. A., Hall, A., Norris, J. R., and Pincus, R.: Low-cloud feedbacks from cloud-controlling  
471 factors: A review, *Shallow Clouds, Water Vapor, Circulation, and Climate Sensitivity*, 135-157,  
472 2017.
- 473 Kollias, Clothiaux, E. E., Miller, M. A., Albrecht, B. A., Stephens, G. L., and Ackerman, T. P.:  
474 Millimeter-wavelength radars - New frontier in atmospheric cloud and precipitation research,  
475 *Bulletin of the American Meteorological Society*, 88, 1608-+, 10.1175/bams-88-10-1608, 2007a.
- 476 Kollias, Clothiaux, E. E., Miller, M. A., Luke, E. P., Johnson, K. L., Moran, K. P., Widener, K. B., and  
477 Albrecht, B. A.: The Atmospheric Radiation Measurement Program cloud profiling radars:  
478 Second-generation sampling strategies, processing, and cloud data products, *Journal of*  
479 *Atmospheric and Oceanic Technology*, 24, 1199-1214, 10.1175/jtech2033.1, 2007b.
- 480 Kollias, Remillard, J., Luke, E., and Szyrmer, W.: Cloud radar Doppler spectra in drizzling stratiform  
481 clouds: 1. Forward modeling and remote sensing applications, *Journal of Geophysical Research-*  
482 *Atmospheres*, 116, 10.1029/2010jd015237, 2011a.
- 483 Kollias, Szyrmer, W., Remillard, J., and Luke, E.: Cloud radar Doppler spectra in drizzling stratiform  
484 clouds: 2. Observations and microphysical modeling of drizzle evolution, *Journal of Geophysical*  
485 *Research-Atmospheres*, 116, 10.1029/2010jd015238, 2011b.
- 486 Kollias, Clothiaux, E. E., Ackerman, T. P., Albrecht, B. A., Widener, K. B., Moran, K. P., Luke, E. P.,  
487 Johnson, K. L., Bharadwaj, N., and Mead, J. B.: Development and applications of ARM millimeter-  
488 wavelength cloud radars, *Meteorological Monographs*, 57, 17.11-17.19, 2016.
- 489 Kollias, Puigdomènech Treserras, B., and Protat, A.: Calibration of the 2007–2017 record of  
490 Atmospheric Radiation Measurements cloud radar observations using CloudSat, *Atmospheric*  
491 *Measurement Techniques*, 12, 4949-4964, 2019.
- 492 Laird, N. F., Ochs Iii, H. T., Rauber, R. M., and Miller, L. J.: Initial precipitation formation in warm  
493 Florida cumulus, *Journal of the atmospheric sciences*, 57, 3740-3751, 2000.
- 494 Leon, D. C., Wang, Z., and Liu, D.: Climatology of drizzle in marine boundary layer clouds based  
495 on 1 year of data from CloudSat and Cloud - Aerosol Lidar and Infrared Pathfinder Satellite  
496 Observations (CALIPSO), *Journal of Geophysical Research: Atmospheres*, 113, 2008.
- 497 Liu, Y., Geerts, B., Miller, M., Daum, P., and McGraw, R.: Threshold radar reflectivity for drizzling  
498 clouds, *Geophysical research letters*, 35, 2008.
- 499 Luke, E. P., and Kollias, P.: Separating Cloud and Drizzle Radar Moments during Precipitation  
500 Onset Using Doppler Spectra, *Journal of Atmospheric and Oceanic Technology*, 30, 1656-1671,  
501 10.1175/jtech-d-11-00195.1, 2013.
- 502 Ma, Y., and Guo, G.: *Support vector machines applications*, Springer, 2014.
- 503 Mace, G. G., Protat, A., Humphries, R. S., Alexander, S. P., McRobert, I. M., Ward, J., Selleck, P.,  
504 Keywood, M., and McFarquhar, G. M.: Southern Ocean cloud properties derived from  
505 CAPRICORN and MARCUS data, *Journal of Geophysical Research: Atmospheres*, 126,  
506 e2020JD033368, 2021.
- 507 Michibata, T., and Takemura, T.: Evaluation of autoconversion schemes in a single model  
508 framework with satellite observations, *Journal of Geophysical Research: Atmospheres*, 120,  
509 9570-9590, 2015.
- 510 Michibata, T., and Suzuki, K.: Reconciling compensating errors between precipitation constraints  
511 and the energy budget in a climate model, *Geophysical Research Letters*, 47, e2020GL088340,  
512 2020.



- 513 Nicholls, S.: The dynamics of stratocumulus: Aircraft observations and comparisons with a mixed  
514 layer model, *Quarterly Journal of the Royal Meteorological Society*, 110, 783-820, 1984.
- 515 Paluch, I., and Lenschow, D.: Stratiform cloud formation in the marine boundary layer, *Journal of*  
516 *the atmospheric sciences*, 48, 2141-2158, 1991.
- 517 Randall, D. A., Coakley, J. A., Fairall, C. W., Kropfli, R. A., and Lenschow, D. H.: OUTLOOK FOR  
518 RESEARCH ON SUB-TROPICAL MARINE STRATIFORM CLOUDS, *Bulletin of the American*  
519 *Meteorological Society*, 65, 1290-1301, 10.1175/1520-0477(1984)065<1290:ofrosm>2.0.co;2,  
520 1984.
- 521 Stephens, G. L.: Cloud feedbacks in the climate system: A critical review, *Journal of climate*, 18,  
522 237-273, 2005.
- 523 Stephens, G. L., L'Ecuyer, T., Forbes, R., Gettelmen, A., Golaz, J. C., Bodas-Salcedo, A., Suzuki, K.,  
524 Gabriel, P., and Haynes, J.: Dreary state of precipitation in global models, *Journal of Geophysical*  
525 *Research: Atmospheres*, 115, 2010.
- 526 Takahashi, H., Suzuki, K., and Stephens, G.: Land-ocean differences in the warm-rain formation  
527 process in satellite and ground-based observations and model simulations, *Quarterly Journal of*  
528 *the Royal Meteorological Society*, 143, 1804-1815, 2017.
- 529 VanZanten, M., Stevens, B., Vali, G., and Lenschow, D.: Observations of drizzle in nocturnal  
530 marine stratocumulus, *Journal of the atmospheric sciences*, 62, 88-106, 2005.
- 531 Vapnik, V., Golowich, S. E., and Smola, A.: Support vector method for function approximation,  
532 regression estimation, and signal processing, *Advances in neural information processing systems*,  
533 281-287, 1997.
- 534 Vial, J., Dufresne, J.-L., and Bony, S.: On the interpretation of inter-model spread in CMIP5 climate  
535 sensitivity estimates, *Climate Dynamics*, 41, 3339-3362, 2013.
- 536 Wang, H., and Feingold, G.: Modeling mesoscale cellular structures and drizzle in marine  
537 stratocumulus. Part I: Impact of drizzle on the formation and evolution of open cells, *Journal of*  
538 *the Atmospheric Sciences*, 66, 3237-3256, 2009.
- 539 Wang, J., Dong, X., and Wood, R.: Aerosol and Cloud Experiments in Eastern North Atlantic (ACE-  
540 ENA) Science Plan, DOE Office of Science Atmospheric Radiation Measurement (ARM) Program ...,  
541 2016.
- 542 Warren, S., Hahn, C., London, J., Chervin, R., and Jenne, R.: Global distribution of total cloud cover  
543 and cloud types over land. NCAR Tech, Note NCAR/TN-273+ STR, 29 pp.+ 200 maps, *Natl. Cent.*  
544 *for Atmos. Res ...*, 1986.
- 545 Warren, S., Hahn, C., London, J., Chervin, R., and Jenne, R.: Global distribution of total cloud cover  
546 and cloud types over ocean. NCAR Tech, Note NCAR/TN-317+ STR, 42 pp.+ 170 maps, 1988.
- 547 Wood: Drizzle in stratiform boundary layer clouds. Part 1: Vertical and horizontal structure,  
548 *Journal of the Atmospheric Sciences*, 62, 3011-3033, 10.1175/jas3529.1, 2005a.
- 549 Wood: Stratocumulus Clouds, *Monthly Weather Review*, 140, 2373-2423, 10.1175/mwr-d-11-  
550 00121.1, 2012.
- 551 Wood, R.: Drizzle in stratiform boundary layer clouds. Part II: Microphysical aspects, *Journal of*  
552 *the Atmospheric Sciences*, 62, 3034-3050, 10.1175/jas3530.1, 2005b.
- 553 Wood, R.: Rate of loss of cloud droplets by coalescence in warm clouds, *Journal of Geophysical*  
554 *Research: Atmospheres*, 111, 2006.



555 Wu, Dong, X., and Xi, B.: Marine boundary layer drizzle properties and their impact on cloud  
556 property retrieval, *Atmospheric Measurement Techniques*, 8, 3555-3562, 10.5194/amt-8-3555-  
557 2015, 2015.

558 Yamaguchi, T., Feingold, G., and Kazil, J.: Stratocumulus to cumulus transition by drizzle, *Journal*  
559 *of Advances in Modeling Earth Systems*, 9, 2333-2349, 2017.

560 Yang, F., Luke, E. P., Kollias, P., Kostinski, A. B., and Vogelmann, A. M.: Scaling of drizzle virga  
561 depth with cloud thickness for marine stratocumulus clouds, *Geophysical Research Letters*, 45,  
562 3746-3753, 2018.

563 Zhang, Z., Song, Q., Mechem, D. B., Larson, V. E., Wang, J., Liu, Y., Witte, M. K., Dong, X., and Wu,  
564 P.: Vertical dependence of horizontal variation of cloud microphysics: observations from the ACE-  
565 ENA field campaign and implications for warm-rain simulation in climate models, *Atmospheric*  
566 *Chemistry and Physics*, 21, 3103-3121, 2021.

567 Zhou, X., Kollias, P., and Lewis, E. R.: Clouds, precipitation, and marine boundary layer structure  
568 during the MAGIC field campaign, *Journal of Climate*, 28, 2420-2442, 2015.

569 Zhu, Z., Kollias, P., Yang, F., and Luke, E.: On the estimation of in-cloud vertical air motion using  
570 radar Doppler spectra, *Geophysical Research Letters*, 48, e2020GL090682, 2021.

571

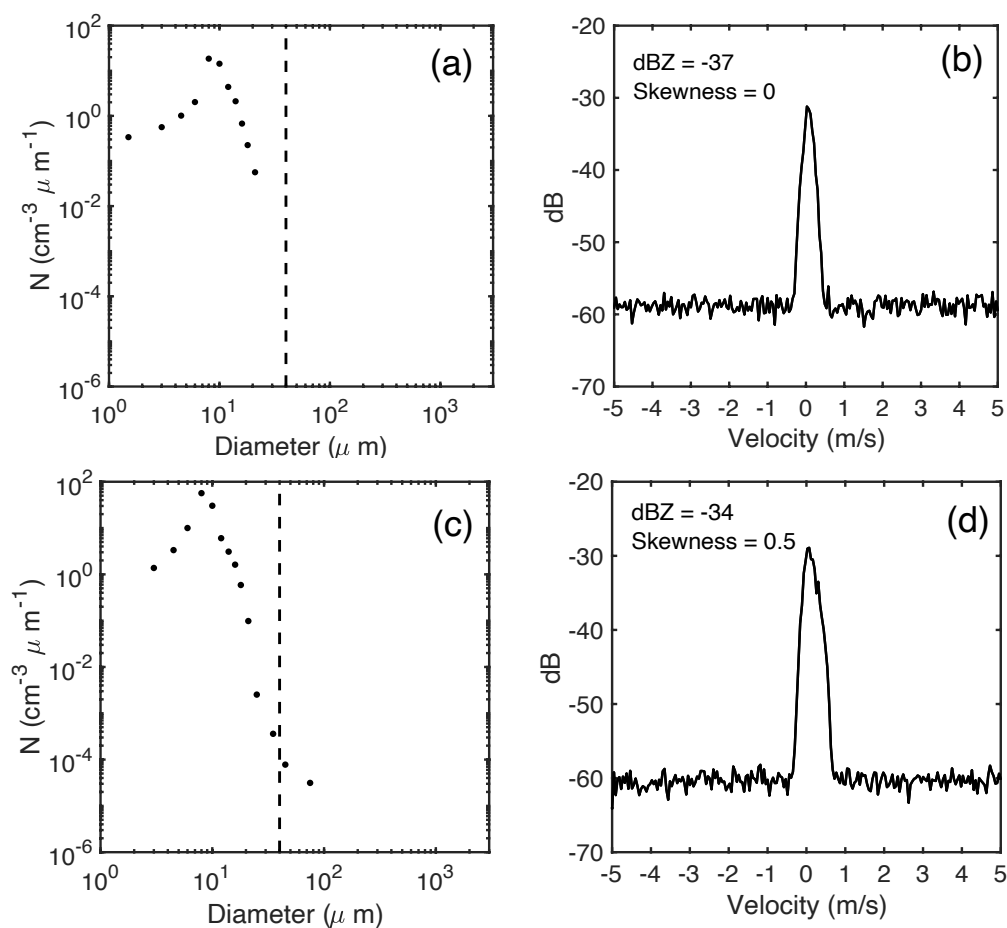
572

573

574



575 Figures and Tables:



576

577 Figure 1: In-situ observed DSD of cloud-only (a) and the corresponding simulated Doppler Radar  
578 spectrum (b), reflectivity and skewness of the spectrum are indicated in the upper left corner. (c)  
579 and (d) are same as (a), (b) but for mixed cloud-drizzle DSD. The dash line in (a), (c) indicates  
580 diameter with  $40 \mu\text{m}$ .

581

582

583

584

585

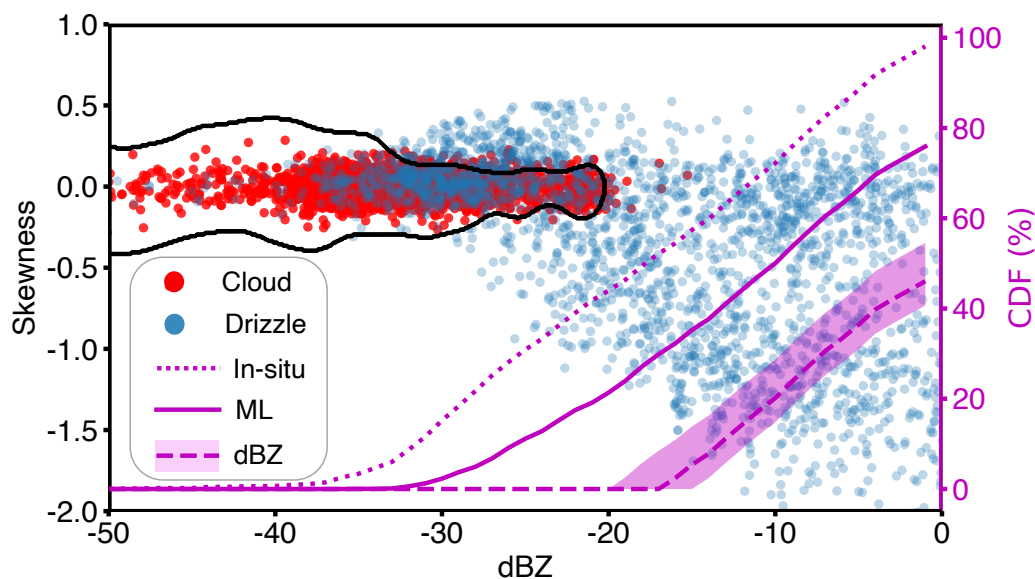
586

587



588

589



590 Figure 2: Distribution of the cloud-only (red points) and mixed cloud-drizzle (blue points) samples  
591 from the in-situ observation over the reflectivity-skewness space. The black line indicates the  
592 classification boundary of cloud/drizzle resolved by Machine Learning algorithm. Right axis  
593 indicates the CDF of all correctly identified drizzly samples as a function of reflectivity by each  
594 method: dotted magenta line is for the in-situ observations, which represents the true value; solid  
595 magenta line is for the ML technique; the magenta shading is for the reflectivity-based technique  
596 with upper boundary using  $\text{dBZ} > -20$  and lower boundary using  $\text{dBZ} > -15$ ; the dashed magenta  
597 line is for the reflectivity-threshold technique with  $\text{dBZ} > -17$ .

598

599

600

601

602

603

604

605

606

607



608 Table 1: Precision(P) and Recall(R) of the drizzle/cloud classification outcome for different  
 609 combination of C and  $\Gamma$ . The dark shaded cell represents the classification performance for the  
 610 selected parameters (C=1,  $\Gamma$ =50) being used in the study.  
 611

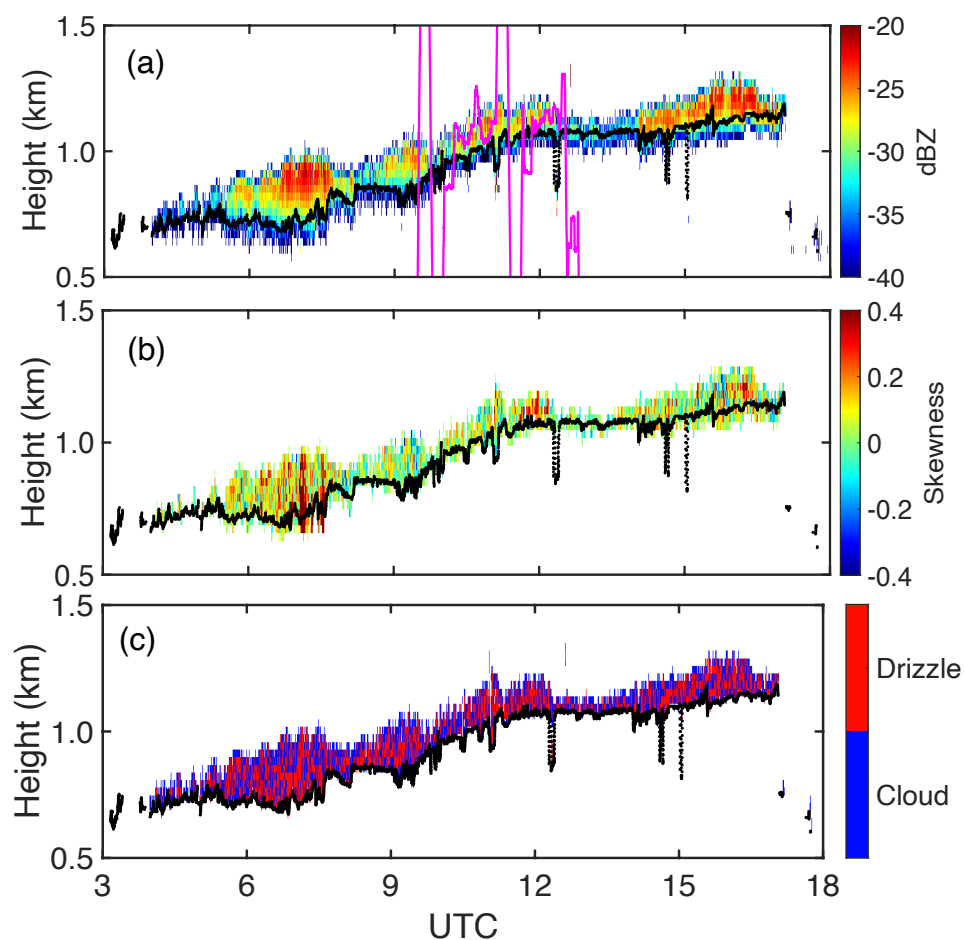
$\Gamma$ C	1	10	50	100	200	500
1	0.99(P)	0.98(P)	0.98(P)	0.98(P)	0.97(P)	0.92(P)
	0.82(R)	0.85(R)	0.85(R)	0.85(R)	0.86(R)	0.87(R)
10	0.99(P)	0.98(P)	0.98(P)	0.98(P)	0.94(P)	0.91(P)
	0.84(R)	0.85(R)	0.85(R)	0.85(R)	0.85(R)	0.86(R)
50	0.99(P)	0.98(P)	0.98(P)	0.97(P)	0.93(P)	0.89(P)
	0.84(R)	0.85(R)	0.85(R)	0.85(R)	0.86(R)	0.87(R)
100	0.99(P)	0.98(P)	0.98(P)	0.96(P)	0.92(P)	0.89(P)
	0.84(R)	0.85(R)	0.84(R)	0.85(R)	0.86(R)	0.87(R)
200	0.98(P)	0.98(P)	0.98(P)	0.95(P)	0.91(P)	0.89(P)
	0.85(R)	0.84(R)	0.84(R)	0.85(R)	0.86(R)	0.87(R)
500	0.98(P)	0.98(P)	0.98(P)	0.94(P)	0.91(P)	0.88(P)
	0.85(R)	0.84(R)	0.85(R)	0.86(R)	0.86(R)	0.87(R)
1000	0.98(P)	0.98(P)	0.97(P)	0.94(P)	0.90(P)	0.88(P)
	0.85(R)	0.84(R)	0.84(R)	0.86(R)	0.86(R)	0.88(R)

612  
 613  
 614  
 615  
 616  
 617  
 618  
 619  
 620  
 621  
 622



623

624



625 Figure 3: Reflectivity (a), skewness (b) and the classification mask (c) on June 30, 2017, at ENA  
626 site. Black line indicates the ceilometer-determined cloud base, magenta line in (a) indicates  
627 altitude track of the aircraft during the observation period.  
628

629

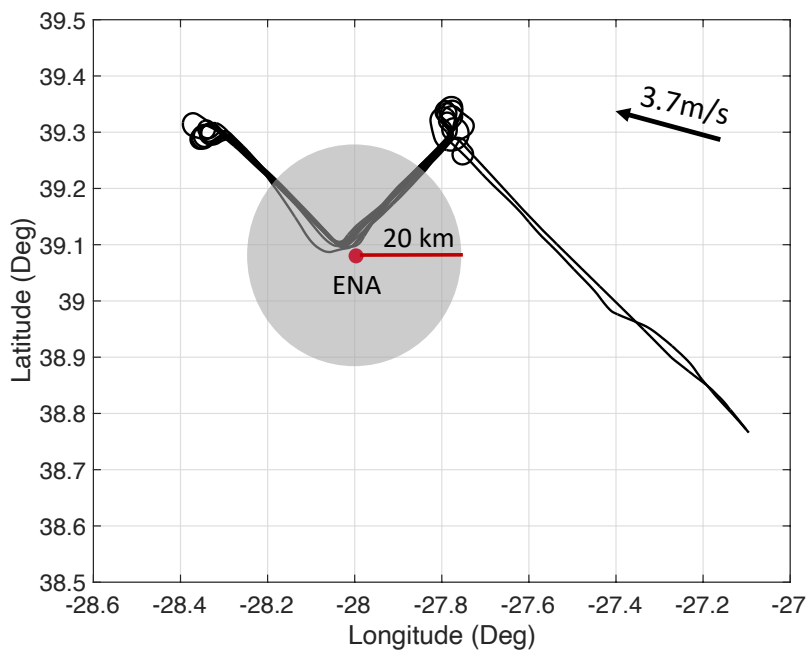
630

631

632



633



634 Figure 4: Aircraft track (black line) during the operational period on June 30, 2017. Shaded circle  
635 indicates the area within 20km around ENA site. The arrow in the upper right corner indicates  
636 mean wind direction and wind velocity in cloud layer during the observational period.  
637

638

639

640

641

642

643

644

645

646

647

648

649

650



651

652

653 Table 2: Selected stratocumulus days in ACE-ENA, MAGIC and MARCUS campaigns.

ARM site	Selected Days
ENA	20170603, 20170604, 20170605, 20170616, 20170617, 20170627, 20170628, 20170630, 20170701, 20170702, 20160703, 20170706, 20170707, 20170709, 20170713, 20170714, 20170715, 20170718, 20170719
MAGIC	20121016, 20121020, 20121030, 20121105, 20130526, 20130604, 20130605, 20130708, 20130709, 20130710, 20130717, 20130720, 20130721, 20130722, 20130729, 20130730, 20130731, 20130804
MARCUS	20180109, 20180110, 20180228, 20180301, 20180322, 20180323

654

655

656

657

658

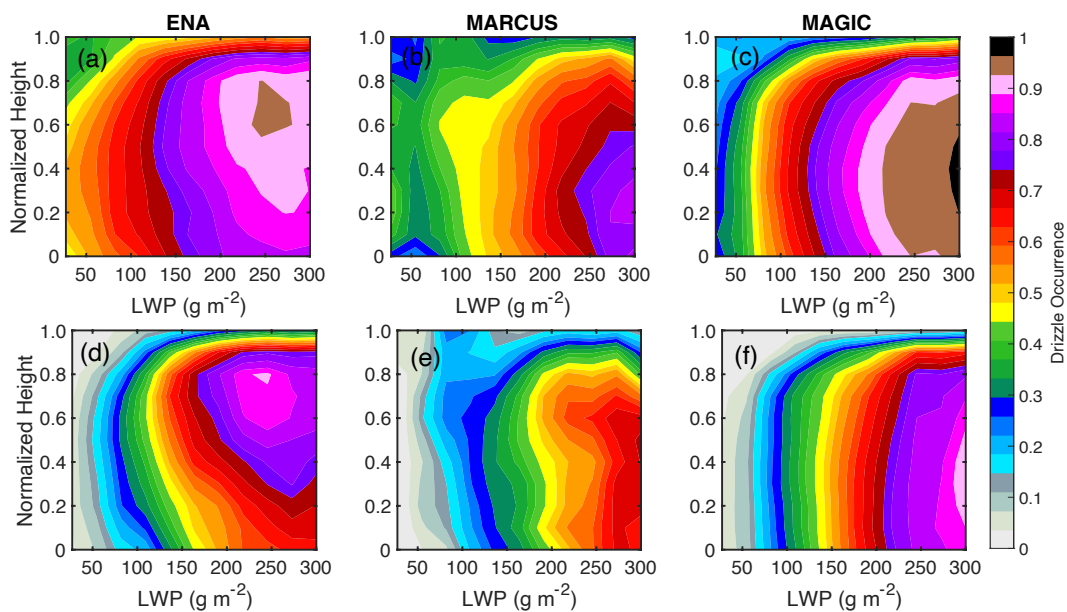
659

660

661

662

663



664

665 Figure 5: Vertical distribution of drizzle occurrence categorized by LWP based on MLA under  
666 ENA (a), MARCUS (b) and MAGIC (c) observational campaigns. (d), (e) and (f) are same as (a),  
667 (b), (c) except the drizzle is detected by dBZA.

668

669

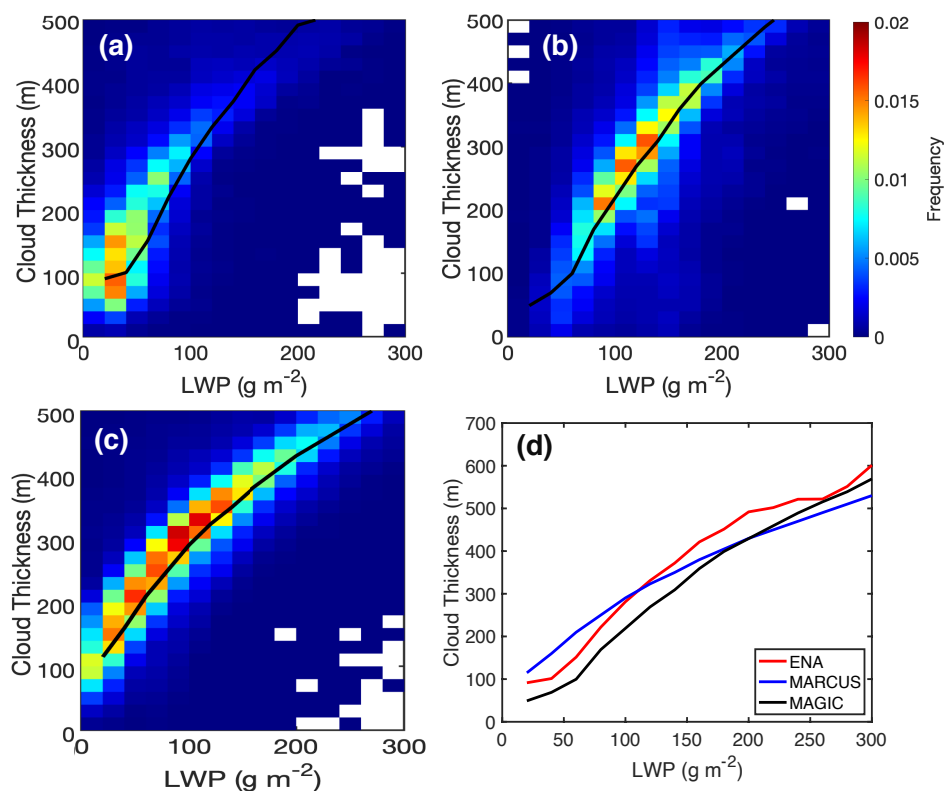
670

671

672

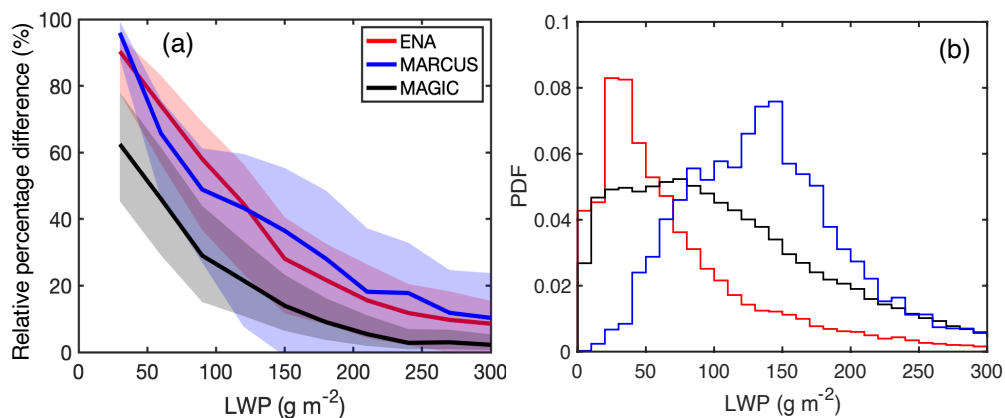
673

674



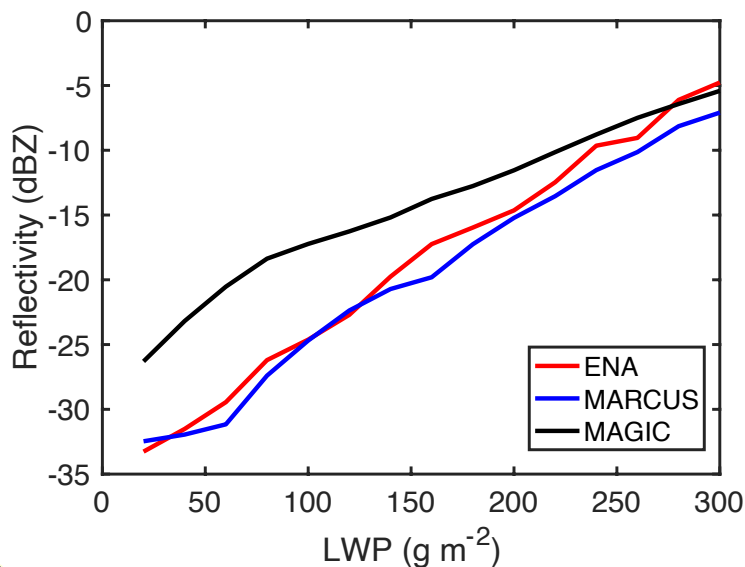
675 Figure 6: Joint histogram of cloud thickness and LWP at three campaigns: (a) ENA, (b) MARCUS  
676 and (c) MAGIC. The black line indicates the mean cloud thickness in each LWP category. For  
677 comparison, the relationship between mean cloud thickness and LWP at three campaigns (black  
678 line in (a),(b),(c) ) are shown in (d).  
679

680  
681  
682  
683  
684  
685  
686  
687  
688



689

690 Figure 7: (a) Relative percentage difference of drizzle detection between the dBZA (dBZ > -17)  
691 and MLA as a function of LWP at ARM observational campaigns: ENA (red line), MARCUS  
692 (blue line) and MAGIC (black line). The shading area indicates same results but with different  
693 reflectivity threshold being used: the upper boundary is for the dBZ > -15 and the lower  
694 boundary is for dBZ > -20. (b) Histogram of the LWP distribution collected at three campaigns:  
695 ENA (red line), MARCUS (blue line) and MAGIC (black line).  
696



697 Figure 8: Mean KAZR reflectivity of the hydrometeor signal as a function of LWP at three  
698 campaigns: ENA (red line), MARCUS (blue line) and MAGIC (black line).  
699